THE DETERMINATION OF LOCAL CORROSION KINETICS USING SCANNING ELECTROCHEMICAL MICROSCOPY

Heming He, Z. Qin, P. Keech, J.J. Noel, Z.F. Ding, D.W. Shoesmith
Department of Chemistry, The University of Western Ontario
London, Ontario, N6A 5B7, Canada

Abstract

The focus of this research is the local corrosion behaviour of a number of hyper-stoichiometric UO_{2+x} electrodes. SECM images and SECM approach curves have been recorded on four well characterized UO_{2+x} specimens with x values of 0.002, 0.011, 0.05, and 0.1 under natural corrosion conditions. Comparison of experimental approach curves to numerically simulated approach curves allowed a determination of the “standard” rate constant for the cathodic reduction of the mediator on the UO_{2+x} surface. Since this reaction is coupled to the anodic dissolution of the UO_{2+x}, it is a measure of fuel corrosion rate. The results suggest that corrosion could be enhanced in non-stoichiomnetric grain boundaries in the fuel.

1. Introduction

The rate of release of radionuclides from spent fuel once contact with groundwater has been established must be considered in safety assessments of a nuclear waste repository. The solubility of UO_2 is extremely small under reducing conditions, but increases by almost 5 orders of magnitude when the UO_2 is oxidized[1]. Consequently, the release of radionuclides will be governed by the corrosion kinetics of the UO_2 matrix which are determined primarily by the repository redox conditions established by the kinetic balance of the anodic and cathodic reactions,

$$\begin{aligned} &UO_2 \rightarrow UO_2^{2+} + 2e^- \\ &[Ox] + 2e^- \rightarrow [\mathrm{Re}\,d] \end{aligned} \qquad (1)$$

An important parameter that can influence both anodic and cathodic reaction kinetics is the degree of non-stoichiomertry of the fuel[2-6]. Non-stoichiometry may exist as a consequence of the original fuel fabrication and sintering process[2-4] and in spent fuel may be generated under normal operating conditions [5] since many fission products have a lower valence than uranium. It may also develop under oxidative conditions after cladding breaches during service or after fuel discharge [6-8].

One Canadian disposal option is deep disposal in a repository in the Canadian Shield. The proposed copper containers are expected to sustain only minimal corrosion, and are unlikely to fail. Therefore, reducing conditions should prevail in a nuclear waste repository, since environmental oxidants (i.e.

dissolved O_2 trapped in porous sealing materials) will be relatively rapidly consumed by waste container corrosion and mineral/biochemical oxidation processes [9]. However, if failure was to occur leading to groundwater entry into the container, the major potential source of oxidants to drive the corrosion would be water radiolysis. The α radiation fields will remain significant for up to 10^5 years [10], UO_2 surfaces could be subject to an oxidizing environment for long periods of time since radiolytic decomposition of water will generate various oxidants (e.g. O_2, O_2^-, OH and H_2O_2) near the surface of the fuel [11-14]. Since H_2O_2 will be the primary radiolytic product, analyses have focused on the interaction of H_2O_2 with UO_2 [15-19].

Scanning electrochemical microscopy (SECM), which combines surface imaging and quantitative approach curve techniques, can be used to detect local reactivity on corroding surfaces. The primary goal of this research is the exploration of the local corrosion behaviour of a number of hyper-stoichiometric UO_{2+x} electrodes. A method has been developed to determine local corrosion kinetics using SECM approach curves in the feedback mode at the corrosion potential on the UO_{2+x} specimens. For spent nuclear fuel analogues (i.e., SIMFUELs), SECM can elucidate the fuel matrix regions of reactivity at the micron scale.

2. Methodology and Theory

2.1 Scanning Electrochemical Microscopy (SECM)

The SECM technique has been described in detail elsewhere [20-29]. Quantitative studies are based on the measurement of the current for oxidation of a redox mediator at an ultramicroelectrode (UME) tip as the tip is either (i) scanned across the substrate (fuel) surface at constant height above the surface (imaging), or (ii) the tip is made to approach the surface at a rate of 1 μm/s and the tip current measured as a function of the tip-substrate separation, d (probe approach curves). The current measured at the UME tip is a measure of the rate of reduction of the mediator on the substrate. In the probe approach curve (PAC) method the tip current approaches zero if the substrate is an insulator, but increases if the mediator is being rapidly reduced on the substrate. Intermediate behavior is a measure of the reactivity of the substrate. In our studies ferrocene methanol (FcMeOH) was used as the mediator since it possesses a similar one electron standard reduction potential to H_2O_2 [1,2] and similar reactivity on the UO_2 surface would be expected[30].

The FcMeOH is oxidized at the UME at a diffusion controlled rate,

$$FcMeOH \underset{UO_{2+x}}{\overset{UME}{\rightleftarrows}} FcMeOH^{+} + e \qquad (2)$$

and the rate of reduction/regeneration of the $FcMeOH^+$ at the UO_{2+x} substrate via the reverse of reaction (2) provides information on the cathodic reduction kinetics at locations on the UO_{2+x} substrate.

2.2 Theory & Simulation Model

To quantify the technique, experimental approach curves were compared to simulated curves. **Figure 1** outlines the procedure used to determine the local corrosion kinetics using this approach. **Figure 2** shows the system boundary definitions that we are going to discuss in our model. Where, c_0, D, k_{s_s} and I_{corr} are the bulk concentration of the FcMeOH, the diffusion coefficient of the FcMeOH / $FcMeOH^+$, reaction rate constant of the substrate, and the corrosion rate, respectively.

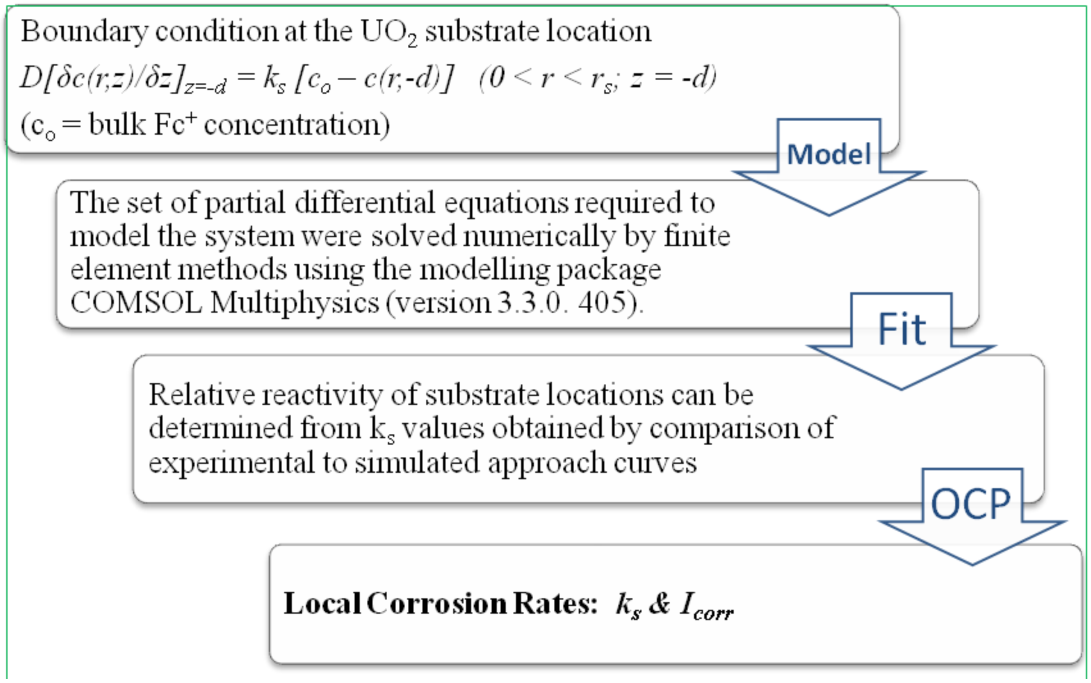

Boundary condition at the UO_2 substrate location
$D[\delta c(r,z)/\delta z]_{z=-d} = k_s\,[c_o - c(r,-d)]$ $(0 < r < r_s;\ z = -d)$
(c_o = bulk Fc^+ concentration)

The set of partial differential equations required to model the system were solved numerically by finite element methods using the modelling package COMSOL Multiphysics (version 3.3.0. 405).

Relative reactivity of substrate locations can be determined from k_s values obtained by comparison of experimental to simulated approach curves

Local Corrosion Rates: k_s & I_{corr}

Figure 1 The procedure and methodology used to determine the local corrosion kinetics using SECM.

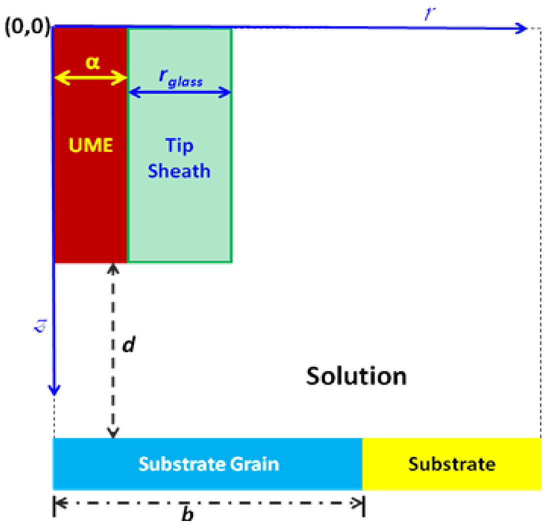

Figure 2 Boundary parameters and geometric description of the SECM model.

Since experiments are conducted in aerated solutions under natural corrosion conditions two possible cathodic reactions are available to drive fuel corrosion; reduction of the mediator and reduction of dissolved O_2. However, the corrosion potential of the fuel sits at a value (-0.3 to 0 V (vs SCE)) at which O_2 reduction is slow and $FcMeOH^+$ reduction is rapid. Consequently, the contribution of O_2 reduction can be ignored and UO_{2+x} corrosion can be considered to be driven by the mediator.

3. Experimental

3.1 Fuel Specimens and Reagents

Four hyper-stoichiometric UO_{2+x} specimens (approximately 5 mm thick and 12mm in diameter), fabricated by Atomic Energy of Canada Limited (AECL) at Chalk River Laboratories (Ontario, Canada), were used. The overall O/U ratios were approximately 2.002, 2.011, 2.05, and 2.1.

Ferrocenemethanol (FcMeOH) was used as received from Aldrich at a concentration of 0.9 mmol/l in 0.1 mol/l sodium chloride. All aqueous solutions were prepared from 18.2 MΩ • cm deionized water purified by Milli-Q deionizer (Millipore Corp.).

3.2 SECM Instrumentation

The detailed description of our homebuilt SECM instrument has been published previously[31]. The four electrode configuration consisted of a 2μm (diameter) Pt UME, the UO_{2+x} sample (substrate), an Ag/AgCl reference electrode and a Pt counter electrode. Single sides of UO_{2+x} electrodes were immersed in a 5 ml Teflon cell filled with a solution containing the redox-active mediator and a supporting electrolyte.

3.3 SECM approach curves and Images.

All approach curves were initiated with the UME tip positioned 100 μm above a specific UO_2 grain. Using the piezo controller, the tip approached the surface of the sample at a rate of 1 μm/s, and the current of the UME as a function of distance was then obtained. SECM feedback imaging was performed by holding the UME at a constant height above the substrate. The UME tip potential is +0.4V vs. SCE.

3.4 Atomic Force Microscopy (AFM)

Atomic force microscope (AFM) was performed on an alpha-SNOW from Wissenschaftliche Instrument and Technology (WITec, Germany). A standard V-shape silicon nitride cantilever with BS-Multi75Al tip (Budget Sensors) was used with a spring constant of 3 N m^{-1} and a resonance frequency of approximately 75Hz. The topographic and frictional images were obtained using contact mode with a resolution of 256×256 points and lateral resolution about 0.2 μm. Software package WITec Project V. 1.88 from WITec was used for the AFM image processing.

4. Results and Discussion

4.1 SECM Images of $UO_{2.1}$ Electrode

Figure 3 shows the SECM images (60×60 μm^2 (**Figure 3**A); 30×30 μm^2 (**Figure 3**B)) recorded on the $UO_{2.1}$ disk electrode at the corrosion potential. The Images show the distribution of sites at which regeneration of the mediator occurs, corresponding to different regions on the surface of the $UO_{2.1}$ electrode. Three distinct regions can be observed: red/yellow, green, and blue regions in the SECM images corresponding to large, medium, and small tip currents, respectively. The image in **Figure 3**A shows only one site yielding a high tip current (red region) within the 60×60 μm^2 area compared to seven such sites in the more magnified area show in **Figure 3**B. The absolute values of current are not necessarily reliable since the constant height mode of SECM imaging captures variations in both reactivity and topography[32].

4.2 SECM Measurements of Reduction Reaction Kinetics at Individual Sites

The problem of topography and a quantitative measurement of electrochemical reactivity can be solved by the approach curve technique. The chosen locations are indicated in **Figure 3**, and the current responses shown in **Figure 4**. If the UME tip approaches an electrochemically inert UO_{2+x} grain, negative feedback due to glass sheath hindered diffusion of the FcMeOH to the UME tip is observed. By contrast, if the mediator is consumed by corrosion of the UO_{2+x}, positive feedback is observed and the value of the current is a measure of the UO_{2+x} corrosivity. The approach curves 1 to 5 are shown in **Figure 4**A and 6 to 8 in **Figure 4**B. The extent of positive feedback is consistent with the color scheme in the images. **Figure 4** also shows the theoretical fit (the open symbols) to the experimental data (solid lines), yielding reliable value of the reactivity rate constant k_s. Deviations of experimental curves from theoretical curves at small separations may be due to contact between the glass insulating sheath and the UO_2 substrate[33] or indicative of a thin layer of water trapped by surface tension as the tip approaches the interface [34]. The best fits are generally obtained in the case of negative feedback. SEM images and EDX spot analyses (data not shown) clearly show that the smooth grains correspond to low degrees of non-stoichiometry leading to low reactivity and negative feedback under OCP conditions. Therefore, the best fitting results are obtained on smooth grains when contact between the UME and the substrate is unlikely.

The approach curves, which are independent of the topography, confirm that the variations in current observed in the SECM images (**Figure 3**) are primarily due to variations in the electrochemical reactivity between grains.

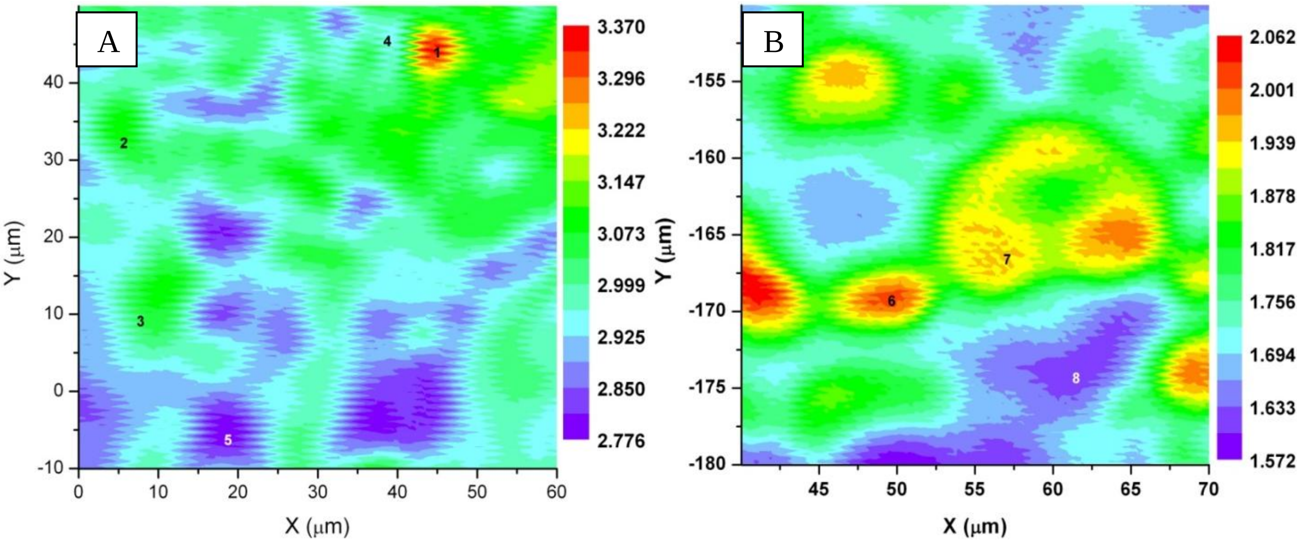

Figure 3 SECM images recorded on a $UO_{2.1}$ disk electrode in 0.1 M NaCl solution containing 0.9 mM FcMeOH under natural corrosion conditions. The images show the feedback currents recorded on the UME after reduction of the mediator on the surface of the electrode. The tip-substrate separation d is ~ 2 μm.

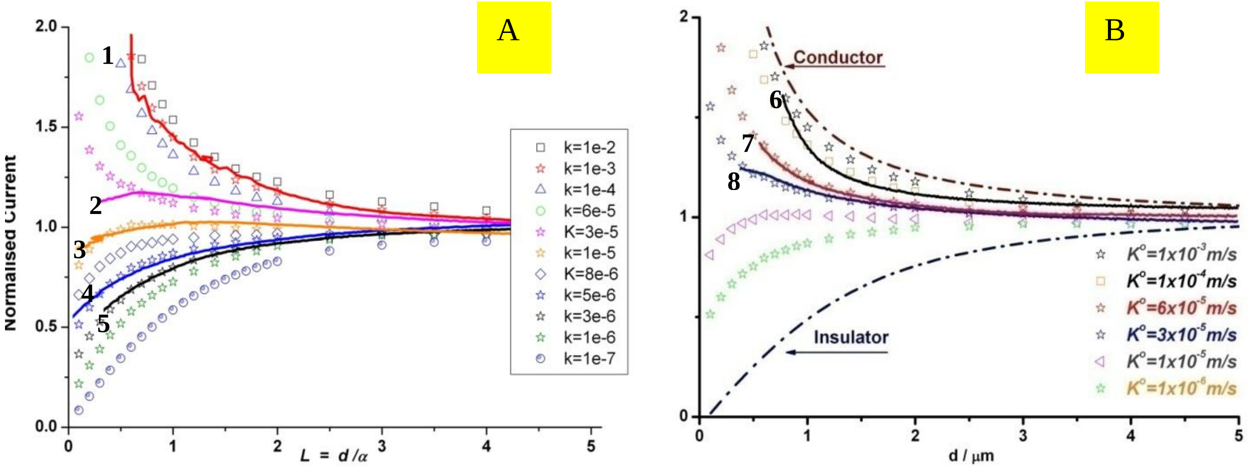

Figure 4 Experimental SECM approach curves (solid lines), obtained in feedback mode using on FcMeOH mediator at a concentration of 0.9 mM on a $UO_{2.1}$ electrode, and the corresponding simulated curves (open symbols). The normalized tip current is ploted versus the normalized tip-substrate separation. The limiting cases of a totally insulating and conducting substrate are shown as dashed lines [35, 36].

4.3 The Influence of the Degree of Non-Stoichimetry on Corrosion Kinetics

SECM experiments were carried out at three other hyper-stoichiometric UO_{2+x} specimens, with x values of 0.002, 0.011, and 0.05, respectively. The standard rate constants are summarized in **Figure 5**, and compared to Raman measurements of the intensity of the O-U fundamental vibrational stretch at 450 cm^{-1}. This Raman feature is a signature of the cubic fluorite structure [37], and decreases in intensity as the degree of non-stoichiometry increases leading to distortion of the cubic lattice.

The spot to spot Raman analyses show that the intensity of this peak varies over a range which increases as the degree of non-stoichiometry of the UO_{2+x} increases. The rate constant determined by SECM also varied considerably from location to location as non-stoichiometry increased. By characterizing the various grain structures visible on the UO_{2+x} surface by Raman spectroscopy it was shown that the rate constant varied with UO_{2+x} lattice structure and was enhanced at more non-stoichiometric locations. This is consistent with the donor / acceptor theory of Presnov and Trunov[38] to explain the catalysis of O_2 reduction on transition metal oxides with *p*-type semiconductivity.

Recent studies indicate that mobile lattice oxygen species are involved in oxidation / reduction processes on oxide surfaces. The clustering of surface Oxygen vacancy defects, which is known to occur in UO_2 as the degree of non-stoichiometry increases[39, 40], leads to high reactivity[41-43]. Therefore, from a structure point of view, fluorite-like hyperstoichiometric UO_{2+x} should possess high reactivity for both cathodic reduction and anodic dissolution reactions.

Consequently, we can conclude that we have measured the corrosion kinetics of the UO_{2+x} through fitting the SECM approach curve for the $FcMeOH^+$ reduction process. This claim is supported by AFM measurements. The left side AFM image in **Figure 6** was recorded on the fresh, un-touched $UO_{2.1}$ surface and clearly shows the presence of smooth grains, mixed flat and facetted features, as well as highly facetted structures. EDX and Raman analyses show that smooth grains are close to stoichiometric while the degree of non-stoichiometry increases with the degree of faceting of the surface features. The right side AFM image in **Figure 6** was obtained on a corroded $UO_{2.1}$ surface immediately after the SECM experiments. The corrosion damage is mainly located on the facetted grains and along grain boundaries suggesting higher corrosion rates in these regions. This is consistent with the SECM images, **Figure 3**, and with the wide range of reactivities determined in the probe approach curves.

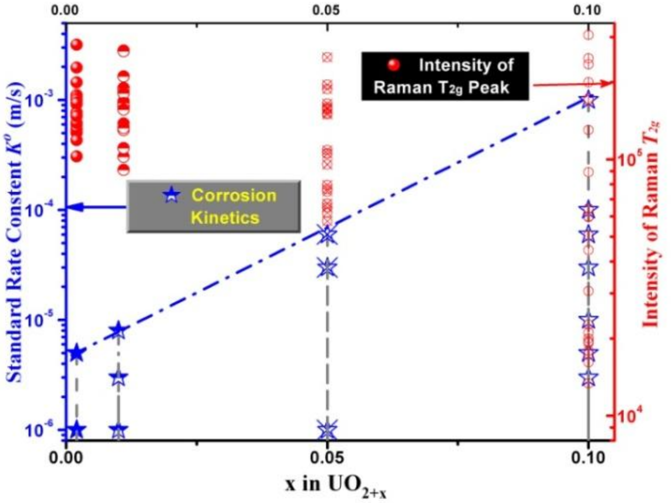

Figure 5 The distribution of the standard rate constants (determined by SECM) and the intensity of the O-U Raman T_{2g} stretch (from Raman mapping) as a function of the degree of non-stoichiometry of the specimens.

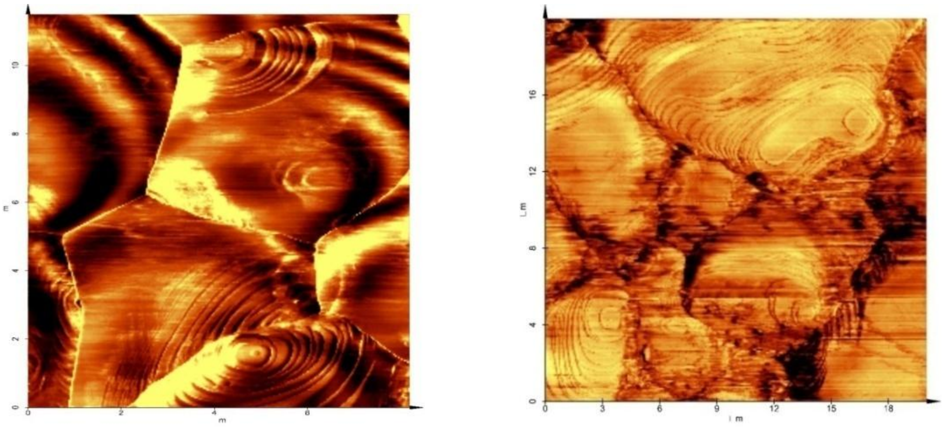

Figure 6 AFM images recorded on a fresh $UO_{2.1}$ electrode surface before SECM experiments (the left side), and at a corroded surface after SECM experiments (right side).

5. Conclusions

A method has been developed to determine cathodic reaction rates and the corrosion kinetics at the individual substrate UO_{2+x} grains in micron scale using SECM measurements. The results quantitatively demonstrate that corrosion rates vary over a broad range, and that this range is determined by the degree of non-stoichiometry of the UO_{2+x} specimens and the diversity of structures on the UO_{2+x} surface. The SECM approach curves and AFM images indicate that the distorted grain structures associated with higher degree of non-stoichiometry show higher corrosion rates. Our results suggest that corrosion could be enhanced at non-stoichiometric sites, probably grain boundaries in the fuel, leading to higher rates for the release of radionuclides from these locations.

Acknowledgements

The authors thank Surface Science Western for Raman and SEM/EDX facilities. This research was funded under the Industrial Research Chair agreement between the Canadian Natural Sciences and Engineering Research Council (NSERC) and the Nuclear Waste Management Organization (NWMO), Toronto, Canada.

References

[1] Shoesmith D.W., Sunder S., and Hocking W.H., *Electrochemistry of Novel Materials*, ed. J. Lipkowski and P.N. Ross. 1994: VCH, New York. pp. 297.
[2] Cobos J., Papaioannou D., Spino J., and Coquerelle M., "Phase characterisation of simulated high burn-up UO_2 fuel", *Journal of Alloys and Compounds*, Vol. 271-273, 1998, pp. 610-615
[3] Abramowski M., Grimes R.W., and Owens S., "Morphology of UO_2", *Journal of Nuclear Materials,* Vol. 275, Iss. 1, 1999, pp. 12-18
[4] Davies J.H., Hoshi E.V., and Zimmerman D.L., "Ramp test behavior of high O/U fuel", *Journal of Nuclear Materials*, Vol. 270, Iss. 1-2, 1999, pp. 87-95
[5] P.G. Lucuta H.M., R.A. Verrall, "Thermal conductivity of hyperstoichimetric SIMFUEL", *Journal of Nuclear Materials*, Vol. 223, 1995, pp. 10
[6] Scott K.T. and Harrison K.T., "Some studies of the oxidation of uranium dioxide", *Journal of Nuclear Materials*, Vol. 8, Iss. 3, 1963, pp. 307-319
[7] Bessonov A.F., Taksis G.A., and Semavin Y.N., "Oxidation of uranium dioxide by heating in air", *Izvestiya Akademii Nauk SSSR, Neorganicheskie Materialy*, Vol. 3, Iss. 6, 1967, pp. 1104-6
[8] Campbell T.K., Gilbert E.R., Thornhill C.K., and Wrona B.J., "Oxidation behavior of spent uranium dioxide fuel", *Nuclear Technology*, Vol. 84, Iss. 2, 1989, pp. 182-95
[9] king F. and Kolar M., "Modelling the consumotion of oxygen by container corrosion and reaction with Fe(II)", *Mat. Res. Soc. Symp. Proc.*, Vol. 412, 1996, pp. 547-554
[10] Sunder S., "Alpha, beta and gamma does rates in water in contact with used CANDU UO_2 fuel," *Atomic Energy of Canada Ltd. Report*, Vol. AECL-11380, COG-95-340, 1995
[11] Christensen H., Sunder S., and Shoesmith D.W., "Oxidation of Nuclear-Fuel (UO_2) by the Products of Water Radiolysis - Development of a Kinetic-Model", *Journal of Alloys and Compounds*, Vol. 213, 1994, pp. 93-99
[12] Wren J.C., Shoesmith D.W., and Sunder S., "Corrosion behavior of uranium dioxide in alpha radiolytically decomposed water", *Journal of the Electrochemical Society*, Vol. 152, Iss. 11, 2005, pp. B470-B481

[13] Sunder S., Shoesmith D.W., and Miller N.H., "Oxidation and dissolution of nuclear fuel (UO_2) by the products of the alpha radiolysis of water", *Journal of Nuclear Materials*, Vol. 244, Iss. 1, 1997, pp. 66-74

[14] Sattonnay G., Ardois C., Corbel C., Lucchini J.F., Barthe M.F., Garrido F., and Gosset D., "Alpha-radiolysis effects on UO_2 alteration in water", *Journal of Nuclear Materials*, Vol. 288, Iss. 1, 2001, pp. 11-19

[15] Goldik J.S., Nesbitt H.W., Noel J.J., and Shoesmith D.W., "Surface electrochemistry of UO_2 in dilute alkaline hydrogen peroxide solutions", *Electrochimica Acta*, Vol. 49, Iss. 11, 2004, pp. 1699-1709

[16] Sunder S., Miller N.H., and Shoesmith D.W., "Corrosion of uranium dioxide in hydrogen peroxide solutions", *Corrosion Science*, Vol. 46, Iss. 5, 2004, pp. 1095-1111

[17] Goldik J.S., Noel J.J., and Shoesmith D.W., "The electrochemical reduction of hydrogen peroxide on uranium dioxide electrodes in alkaline solution", *Journal of Electroanalytical Chemistry*, Vol. 582, Iss. 1-2, 2005, pp. 241-248

[18] Goldik J.S., Noel J.J., and Shoesmith D.W., "The effects of simulated fission products in the reduction of hydrogen peroxide on simulated nuclear fuel electrodes", *Journal of the Electrochemical Society*, Vol. 153, Iss. 9, 2006, pp. E151-E159

[19] Goldik J.S., Noel J.J., and Shoesmith D.W., "Surface electrochemistry of UO_2 in dilute alkaline hydrogen peroxide solutions - Part II. Effects of carbonate ions", *Electrochimica Acta*, Vol. 51, Iss. 16, 2006, pp. 3278-3286

[20] Bard A.J., Mirkin M.V., Unwin P.R., and Wipf D.O., "Scanning electrochemical microscopy. 12. Theory and experiment of the feedback mode with finite heterogeneous electron-transfer kinetics and arbitrary substrate size", *J. Phys. Chem.*, Vol. 96, Iss. 4, 1992, pp. 1861-1868

[21] Mirkin M.V. and Horrocks B.R., "Electroanalytical measurements using the scanning electrochemical microscope", *Analytica Chimica Acta* Vol. 406 2000, pp. 119-146

[22] Mirkin M.V., Richards T.C., and Bard A.J., "Scanning electrochemical microscopy. 20. Steady-state measurements of the fast heterogeneous kinetics in the ferrocene/acetonitrile system", *Journal of Physical Chemistry*, Vol. 97, Iss. 29, 1993, pp. 7672-7677

[23] Mirkin M.V. and Sun P. *SECM measurements of rapid electron transfer kinetics across self-assembled molecular monolayers*. in *Meeting Abstracts*. 2005.

[24] Unwin P.R. and Bard A.J., "Scanning electrochemical microscopy. 9. Theory and application of the feedback mode to the measurement of following chemical reaction rates in electrode processes", *J. Phys. Chem.*, Vol. 95, Iss. 20, 1991, pp. 7814-7824

[25] Unwin P.R. and Bard A.J., "Scanning electrochemical microscopy. 14. Scanning electrochemical microscope induced desorption: a new technique for the measurement of adsorption/desorption kinetics and surface diffusion rates at the solid/liquid interface", *J. Phys. Chem.*, Vol. 96, Iss. 12, 1992, pp. 5035-5045

[26] Wei C. and Bard A.J., "Scanning Electrochemical Microscopy. 31. Application of SECM to the Study of Charge Transfer Processes at the LiquidLiquid Interface", *J. Phys. Chem.* , Vol. 99, 1995, pp. 16033-16042

[27] Zhou F., Unwin P.R., and Bard A.J., "Scanning electrochemical microscopy. 16. Study of second-order homogeneous chemical reactions via the feedback and generation/collection modes", *J. Phys. Chem.*, Vol. 96, Iss. 12, 1992, pp. 4917-4924

[28] Zoski C.G., Aguilar J.C., and Bard A.J., "Scanning Electrochemical Microscopy. 46. Shielding Effects on Reversible and Quasireversible Reactions", *Anal. Chem.*, Vol. 75, Iss. 13, 2003, pp. 2959-2966

[29] Zoski C.G., Liu B., and Bard A.J., "Scanning Electrochemical Microscopy: Theory and Characterization of Electrodes of Finite Conical Geometry", *Anal. Chem.*, Vol. 76, Iss. 13, 2004, pp. 3646-3654

[30] Ekeroth E. and Jonsson M., "Oxidation of UO_2 by radiolytic oxidants", *Journal of Nuclear Materials*, Vol. 322, Iss. 2-3, 2003, pp. 242-248

[31] Zhu R. and Ding Z., "Enhancing image quality of scanning electrochemical microscopy by improved probe fabrication and displacement", *Can. J. Chem.*, Vol. 83, Iss. 10, 2005, pp. 1779-1791

[32] Kottke P.A. and Fedorov A.G., "Advective and transient effects in combined AFM/SECM operation", *J. Electroanal. Chem.*, Vol. 583, Iss. 2, 2005, pp. 221-231

[33] Sun P. and Mirkin M.V., "Scanning Electrochemical Microscopy with Slightly Recessed Nanotips", *Anal. Chem.*, Vol. 79, Iss. 15, 2007, pp. 5809-5816

[34] Cannan S., Zhang J., Grunfeld F., and Unwin P.R., "Scanning Electrochemical Microscopy (SECM) Studies of Oxygen Transfer across Phospholipid Monolayers under Surface Pressure Control: Comparison of Monolayers at Air/Water and Oil/Water Interfaces", *Langmuir*, Vol. 20, Iss. 3, 2004, pp. 701-707

[35] Mirkin M.V., Fan F.R.F., and Bard A.J., "Scanning electrochemical microscopy. Part 13. Evaluation of the tip shapes of nanometer size microelectrodes", *J. Electroanal. Chem.*, Vol. 328, Iss. 1-2, 1992, pp. 47-62

[36] Shao Y. and Mirkin M.V., "Probing Ion Transfer at the Liquid/Liquid Interface by Scanning Electrochemical Microscopy (SECM)", *J. Phys. Chem. B*, Vol. 102, Iss. 49, 1998, pp. 9915-9921

[37] Senanayake S.D., Waterhouse G.I.N., Chan A.S.Y., Madey T.E., Mullins D.R., and Idriss H., "The reactions of water vapour on the surfaces of stoichiometric and reduced uranium dioxide: A high resolution XPS study", *Catalysis Today*, Vol. 120, Iss. 2, 2007, pp. 151-157

[38] Presnov V.A. and Trunov A.M., *Electrokhimiya*, Vol. 11, 1975, pp. 77

[39] Catlow C.R.A., "Point Defect and Electronic Properties of Uranium Dioxide", *Proceedings of the Royal Society of London. Series A, Mathematical and Physical Sciences*, Vol. 353, Iss. 1675, 1977, pp. 533-561

[40] Allen G.C. and Tempest P.A., "Ordered Defects in the Oxides of Uranium", *Proceedings of the Royal Society of London. Series A, Mathematical and Physical Sciences,*, Vol. 406, , Iss. 1831, Aug. 8, 1986, pp. 325-344.

[41] Esch F., Fabris S., Zhou L., Montini T., Africh C., Fornasiero P., Comelli G., and Rosei R., "Electron Localization Determines Defect Formation on Ceria Substrates", *Science*, Vol. 309, Iss. 5735, 2005, pp. 752-755

[42] Campbell C.T. and Peden C.H.F., "Oxygen Vacancies and Catalysis on Ceria Surfaces", *Science*, Vol. 309, Iss. 5735, 2005, pp. 713-714

[43] Gritschneder S. and Reichling M., "Structural elements of CeO_2(111) surfaces", *Nanotechnology*, Vol. 18, Iss. 4, 2007, pp. 044024 (6pp)